THE JOURNAL OF BIOLOGICAL CHEMISTRY VOL. 291, NO. 38, pp. 19813–19825, September 16, 2016

Cell Damage in Light Chain Amyloidosis

FIBRIL INTERNALIZATION, TOXICITY AND CELL-MEDIATED SEEDING[*] [S]

Received for publication, May 6, 2016, and in revised form, July 15, 2016 Published, JBC Papers in Press, July 26, 2016, DOI 10.1074/jbc.M116.736736

Marta Marin-Argany[‡], Yi Lin[§¶], Pinaki Misra[‡], Angela Williams[‖], Jonathan S. Wall[‖], Kyle G. Howell[**], Laura R. Elsbernd[‡‡], Megan McClure[§§], and Marina Ramirez-Alvarado[‡ ‡‡1]

From the Departments of [‡]Biochemistry and Molecular Biology and [‡‡]Immunology, the [§]Division of Hematology, the [¶]Human Cell Therapy Lab, Division of Transfusion Medicine, the [**]Department of Microscopy and the Cell Analysis Core Facility, and the [§§]Department of Radiology, Mayo Clinic, Rochester, Minnesota 55905 and the [‖]Departments of Medicine and Radiology, the University of Tennessee Graduate School of Medicine, Knoxville, Tennessee 37920

Light chain (AL) amyloidosis is an incurable human disease characterized by the misfolding, aggregation, and systemic deposition of amyloid composed of immunoglobulin light chains (LC). This work describes our studies on potential mechanisms of AL cytotoxicity. We have studied the internalization of AL soluble proteins and amyloid fibrils into human AC16 cardiomyocytes by using real time live cell image analysis. Our results show how external amyloid aggregates rapidly surround the cells and act as a recruitment point for soluble protein, triggering the amyloid fibril elongation. Soluble protein and external aggregates are internalized into AC16 cells via macropinocytosis. AL amyloid fibrils are shown to be highly cytotoxic at low concentrations. Additionally, caspase assays revealed soluble protein induces apoptosis, demonstrating different cytotoxic mechanisms between soluble protein and amyloid aggregates. This study emphasizes the complex immunoglobulin light chain-cell interactions that result in fibril internalization, protein recruitment, and cytotoxicity that may occur in AL amyloidosis.

Light chain (AL)[2] amyloidosis is a protein misfolding disease characterized by extracellular deposition of immunoglobulin light chains (LC) as amyloid fibrils. LC proteins are comprised of two distinct domains: the variable (V_L) and constant (C_L) domains (also called LC full-length (FL) protein to differentiate with the V_L domain). In patients with AL amyloidosis, the LC aggregate and deposit in vital organs, causing organ failure and death (1). The factors governing deposition in individual tissues are unknown. Patients with cardiac AL amyloidosis have the worst prognosis, with a median survival of less than a year (2, 3).

The finding that the V_L was the primary component of amyloid fibrils influenced previous biophysical studies (4, 5). Recent proteomic studies have demonstrated that amyloid deposits are likely heterogeneous in nature and can be formed by FL, V_L, C_L, or mixtures of all types of LC fragments (6–8). Thermodynamic studies proposed a stabilizing role for the $\lambda 3C_L$ domain in the stability and a modulating effect on fibril formation (9). Recently, our laboratory has demonstrated that the κC_L domain modulates the amyloid formation reaction but has no effect on the stability of the protein (10).

Soluble monoclonal LC, isolated from patients with amyloidosis, can impair rat cardiomyocyte function (11) and induce apoptotic events in mouse cardiomyocytes (12, 13). Also, urine-derived LC can be internalized into primary rat cardiac fibroblasts (14) and primary human renal mesangial cells (15) through a pinocytic pathway (16) or via receptor, clathrin-mediated mechanisms, respectively (15).

Within the amyloid field, it is widely accepted that oligomeric species are potentially more toxic than mature fibrils (17–20). However, toxicity associated with amyloid fibrils may also be pathologically relevant. Engel *et al.* (21) described a mechanism in which growth of islet amyloid associated polypeptides fibrils is responsible for membrane disruption. Gharibyan *et al.* (22) demonstrated that lysozyme amyloid fibrils induce cell death. LC amyloid deposits are proposed to be the most common cause of amyloid cardiomyopathy (2, 23); λ6 LC amyloid fibrils, but not the soluble precursor proteins, severely impair AC10 cardiomyocyte metabolism (24).

Our laboratory has compared the internalization rates of recombinant LC proteins. Levinson *et al.* (25) demonstrated that all proteins studied shared a common internalization pathway into lysosomal compartments.

In the present work, we have studied the mechanism of internalization into human AC16 cardiomyocytes of an amyloidogenic AL-09 protein and the non-amyloidogenic control κI O18/O8 (IGKV 1–33) (hereafter called κI for simplicity). Both soluble and fibrillar species and the FL and V_L proteins have been compared by using real time live cell image analysis. Using endocytic inhibitors, we elucidated the mechanism of internalization of soluble LC and fibrils. Cell-mediated seeding of FL and V_L was shown by incubating preformed aggregates with soluble protein in the presence of AC16 cardiomyocytes. Soluble protein and, to a larger extent, fibrillar aggregates induce

[*] This work was supported by National Institutes of Health Grants R01 GM071514 (to M. R.-A.) and R01 DK079984 (to J. S. W.) and by Dr. Morie Gertz, the Seidler Professorship, and the Mayo Foundation. The authors declare that they have no conflicts of interest with the contents of this article. The content is solely the responsibility of the authors and does not necessarily represent the official views of the National Institutes of Health.
[S] This article contains supplemental Figs. S1–S3.
[1] To whom correspondence should be addressed: Dept. of Biochemistry and Molecular Biology, College of Medicine, Mayo Clinic, 200 First St. SW, Rochester, MN 55905. Tel.: 507-284-2705; E-mail: ramirezalvarado.marina@mayo.edu.
[2] The abbreviations used are: AL, amyloidogenic light chain; LC, immunoglobulin light chain(s); FL, full-length; CL, constant domain; VL, variable domain; OG, Oregon Green; RFP, red fluorescent protein; DYN, Dynasore; GEN, genistein; CYT, cytochalasin D; ThT, thioflavin T.

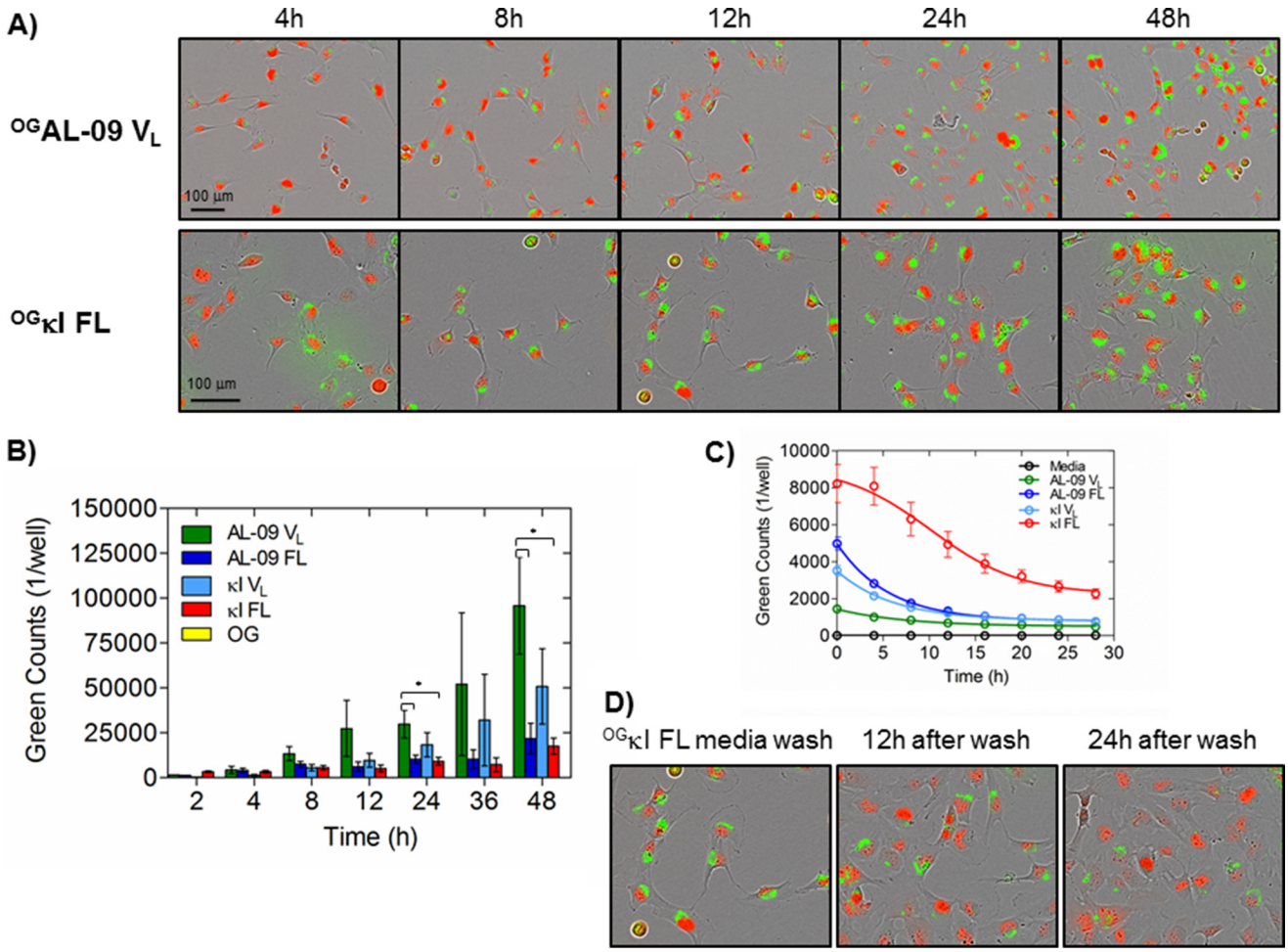

FIGURE 1. **LC soluble proteins internalize into AC16 cells.** *A*, representative images of RFP-AC16 cells incubated with 1 μM ^{OG}AL-09 V_L and $^{OG}\kappa$I FL proteins showing cell associated green fluorescence increasing every 4 h and localization in perinuclear regions. Because κI FL has more OG binding sites than AL-09 V_L, κI FL appears more fluorescent than AL-09 V_L. Green fluorescence signal was normalized for a correct quantification and comparison. *B*, quantification of soluble AL protein internalization over time. V_L domains internalize faster than FL proteins. Also, both V_L and FL AL-09 proteins internalize faster than the both κI germlines. *C*, quantification of decrease in protein-associated fluorescence emission. Internalized AL soluble protein fluorescence decreases rapidly after the ^{OG}LC-rich medium is replaced with ^{OG}LC-free medium. *D*, representative images of AC16 cells with decreasing amounts of intracellular $^{OG}\kappa$I FL protein fluorescence after 12 and 24 h of ^{OG}LC-rich medium wash. Green fluorescence intensities were normalized for each protein as a function of their degree of labeling. Samples were set up in triplicate in four independent assays ($n = 4$) with the average values and *error bars* as means ± S.E. *, two-tailed *t* test; *p* value < 0.05.

cytotoxicity in cultured AC16 cells; however, the toxic effect was mediated via different mechanisms.

Our study highlights the complex aspects behind LC internalization and cytotoxicity in AL amyloidosis, underlying the importance of the amyloid fibrils in the process. Our experiments model the cellular mechanisms that may occur during the early events in AL amyloidosis.

Results

Soluble LC Internalize into Human Cardiomyocytes in a Size-dependent Manner—Using real time live cell imaging, we followed the kinetics of soluble protein internalization in live cells without external perturbation. Fig. 1*A* shows that the Oregon Green (OG) conjugated AL-09 V_L (^{OG}AL-09 V_L) and κI FL ($^{OG}\kappa$I FL) proteins associate with and are increasingly internalized into human AC16 cardiomyocytes over a 48-h period. As shown in Fig. 1*B*, all OG-labeled soluble proteins tested appeared inside cells after 4 h of incubation at 37 °C and substantially increased over time. Both V_L domains show a higher rate of internalization over time compared with the FL proteins as can be observed in Fig. 1*B*. After 12 h, ^{OG}LC soluble protein was found in the majority of the cardiomyocytes imaged (Fig. 1*A*). As a control, unconjugated OG was added to cell cultures and did not enter the cells. We do not see soluble protein accumulation on the plasma membrane. The internalized protein is predominantly accumulated and localized in perinuclear compartments as evidenced by confocal microscopic analysis (supplemental Fig. S1), in agreement with the co-localization studies conducted previously with HL-1 mouse cardiomyocytes (25).

To determine the importance of the C_L on the internalization rates, we compared the kinetics of internalization of FL proteins with their V_L counterparts. Red fluorescent protein (RFP)-AC16 cells were incubated with 1 μM of either FL or V_L domains. For proper comparison, the fluorescence intensity of each protein was normalized by its degree of OG labeling (see "Experimental Procedures"). Fig. 1*B* shows that V_L domains have higher amounts of intracellular protein than FL proteins, suggesting a size-dependent correlation with the rate of inter-

nalization. As shown in Table 1, the amyloidogenic protein AL-09 internalizes faster than the germline κI, for both V_L and FL proteins (although the differences are not statistically significant between AL-09 V_L and κI V_L; AL-09 FL and κI FL, see Table 1 for details). For a correct quantification of the protein internalized, ^{OG}LC-rich medium was replaced with protein-free medium before each live cell imaging time point. After 24 h, the ^{OG}LC medium was replaced with medium alone. We followed the trafficking of the fluorescent protein for an extended period of time. We observed substantially decreased intracellular protein fluorescence over time (Fig. 1, *C* and *D*). We ruled out fluorescence quenching or signal degradation as a potential explanation for the reduction of fluorescence because we observed intracellular fluorescence in cells that have been incubated with ^{OG}LC for 48 h (see "Experimental Procedures").

TABLE 1

LC protein internalization rate

The samples were set up in triplicate in four independent assays ($n = 4$). The data on the table are means ± S.E. determined by two-tailed *t* test. The *p* values are <0.05 between AL-09 V_L and AL-09 FL and between AL-09 V_L and κI FL.

LC protein	Internalization rate
	counts/h
AL-09 V_L	1995.95 ± 562
AL-09 FL	455.06 ± 175.16
κI V_L	1059.32 ± 436.90
κI FL	367.66 ± 94.74

We suggest that the internalized protein leaves the AC16 cells via an exocytosis mechanism. Extracellular fluorescence is diffused and not detected by our imaging system.

Protein Internalization Is Mediated by a Macropinocytic Mechanism—To understand the mechanism of LC internalization, studies with endocytosis inhibitors were performed. Before ^{OG}LC proteins were added, RFP-AC16 cells were treated with: Dynasore (DYN), a dynamin-GTPase inhibitor that blocks clathrin-mediated endocytosis (26–28); tetradecyl trimethyl ammonium bromide (MiTMAB), a dynamin inhibitor that specifically blocks receptor-mediated endocytosis in non-neuronal cells (29, 30); genistein (GEN), a GTPase inhibitor that prevents the clathrin-independent endocytic pathway; and cytochalasin D (CYT), an inhibitor of actin polymerization required for membrane-ruffling and macropinosome formation (31).

After 28 h of cell treatment with 50 μM DYN, both V_L domains (AL-09 and κI) decrease their uptake over 25% in comparison with the untreated controls at the same time point (Fig. 2, *A* and *B*), whereas the FL protein internalization remained practically unaltered (Fig. 2, *C* and *D*). Cell treatment with 10 μM MiTMAB decreased the internalization for both V_L and FL proteins. The effect reached 60% inhibition for both germline κI proteins (Fig. 2, *B* and *D*), and ~50% inhibition for both AL-09 proteins (Fig. 2, *A* and *C*, *green bars*). In contrast, 50 μM

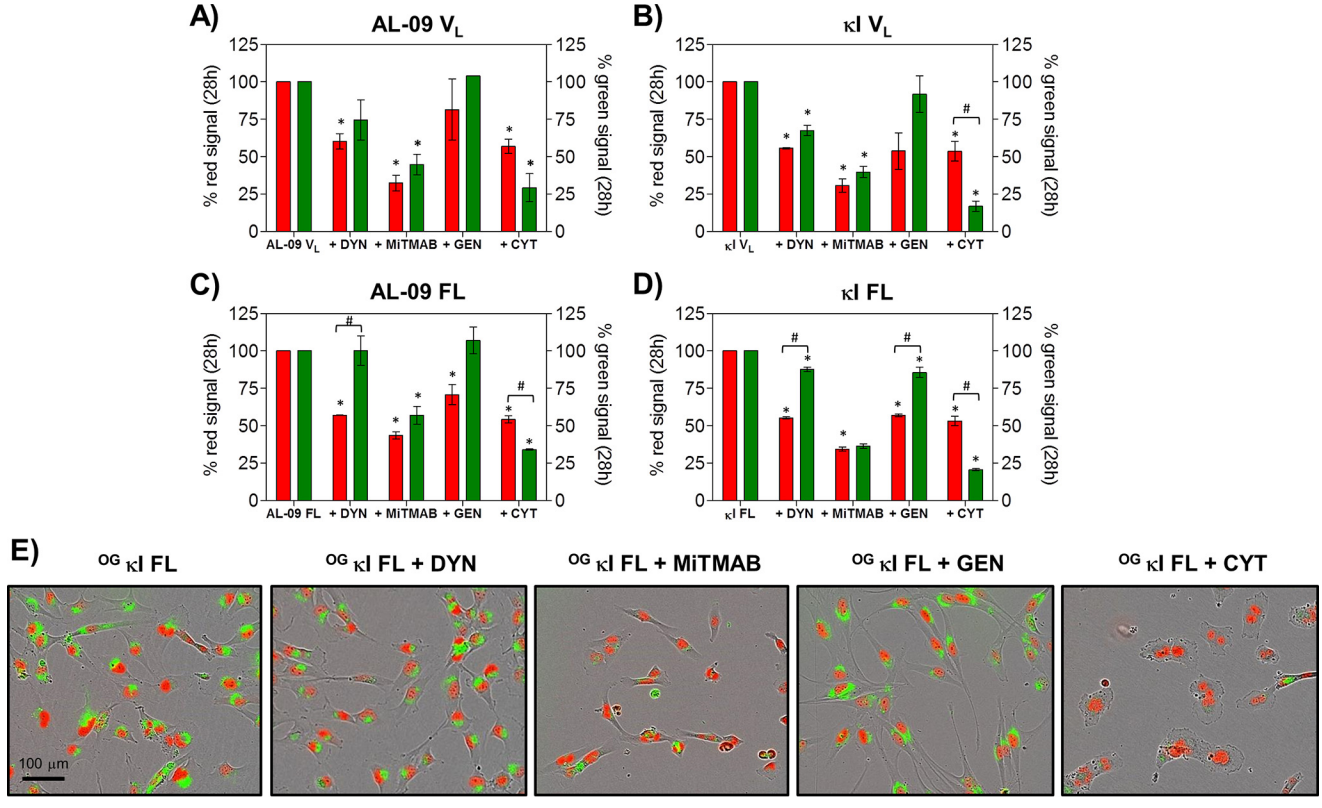

FIGURE 2. **Macropinocytic pathway for soluble protein internalization.** *A–D*, quantification of 1 μM soluble protein internalization (*green bars*) and AC16 viability (*red bars*) after 28 h of co-incubation in presence of 50 μM DYN, 10 μM MiTMAB, 50 μM GEN, and 1 μM CYT. All inhibitors decreased cell viability by ~50%. DYN, MiTMAB, and GEN had no significant effect on protein internalization, whereas CYT reduced protein fluorescence by 75% in all cases. *E*, representative images of AC16 cells with intracellular ^{OG}κI FL protein after 28 h of incubation. DYN and GEN show similar green fluorescence intensity compared with no treatment. MiTMAB shows a slight reduction in fluorescence, which correlates with the decreased number of cells. CYT clearly shows a significant reduction of intracellular green signal, which indicates the inhibition of a macropinocytic mechanism. Samples were set up in triplicate in three independent assays ($n = 3$) with the average values and *error bars* as means ± S.E. *, two-tailed *t* test; *p* value < 0.05 with respect to the corresponding controls. #, two-tailed *t* test; *p* value < 0.05 between values at same condition.

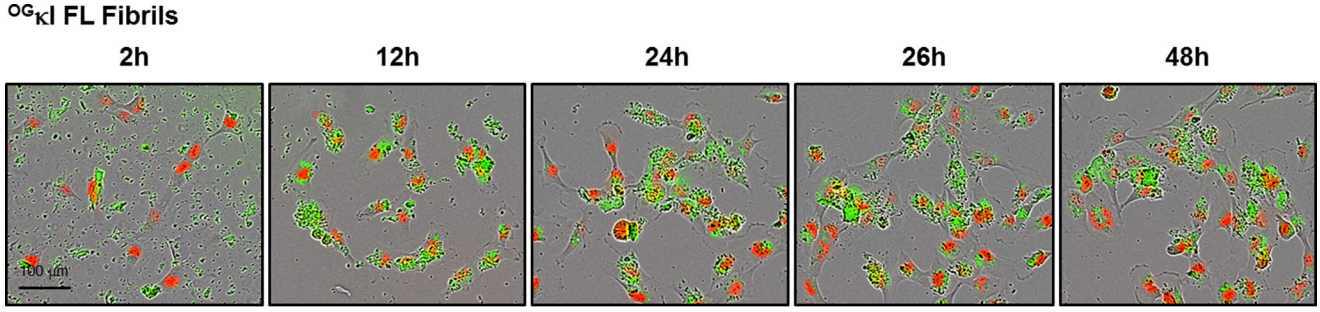

FIGURE 3. **LC fibrils interact with cell membranes and promote cell clustering.** Shown is a sequence of representative images of AC16 cells incubated with 1 μM $^{OG}\kappa$I FL fibrils showing external aggregates surrounding the cardiomyocytes and promoting cell clustering increased over time.

GEN does not show any substantial effect on the internalization of the four variants compared with the untreated cells (Fig. 2, *A–D*). Relative to the respectively cell number, cell treatment with DYN and GEN increased the uptake of FL proteins. Cells treated with 1 μM CYT significantly reduced the internalization rates to values less than 25% for both V_L and κI FL proteins and ~30% for AL-09 FL protein (Fig. 2, *A–D*). The images in Fig. 2*E* show changes in cell morphology and viability caused by treatment with the inhibitors in the presence of $^{OG}\kappa$I FL. The observation that DYN and MiTMABs were causing a decrease in the cell growth could be interpreted as an inhibitory effect. CYT also decreases the cell viability by 50%; the green signal reduction is not completely related to the reduced number of cells in the wells but rather to the inhibition of the internalization process. When we compared the quantified cardiomyocyte viability (percentage of red cells) (Fig. 2, *A–D*, *red bars*) with the internalized protein (Fig. 2, *A-D*, *green bars*), we were able to assess the real effect of each inhibitor on the AL internalization process. As shown in Fig. 2*E* with $^{OG}\kappa$I FL protein, for example, the green signal inside the cells is practically nonexistent in the presence of CYT. MiTMAB treatment, to a lesser extent, also decreased the protein internalization.

External Fibrillar Aggregates Interact with Cell Membranes and Recruit Soluble Protein—After examining the endocytic pathway for soluble LC protein, we sought to describe the behavior of amyloid fibrils incubated with AC16 cardiomyocytes. OG-labeled fibrils composed of κI FL were added to RFP-AC16 cells, and their growth was monitored over 48 h (Fig. 3). Unlike LC soluble protein, external aggregates show a strong attraction to the plasma membrane. Fibrils rapidly surrounded the cardiomyocytes and promoted cell clustering and confined cell growth. Fig. 4 demonstrates a significant reduction in $^{OG}\kappa$I FL fibril internalization by CYT, indicating that fibril uptake also occurs predominantly via macropinocytosis. As seen for soluble protein, MiTMAB treatment slightly decreased the intracellular green signal, suggesting a possible secondary pathway.

We then asked whether AL fibrils could compete with and reduce AC16 internalization of the soluble protein. Conjugation with OG does not affect the LC fibril morphology, as observed by EM (data not shown). Fig. 5 shows $^{OG}\kappa$I FL protein as a representative example of the competition experiments in which we incubated each of the species (soluble protein, amyloid fibrils, or their co-incubation) with the cells. Soluble $^{OG}\kappa$I FL protein internalized and localized in perinuclear compartments as described above (Fig. 5*A*). When cells were incubated with $^{OG}\kappa$I FL or non-labeled fibrils, fibrils were observed associated with the cells surface. Fibril labeling highlights the internalized and perinuclear fibrils (Fig. 5, *B* and *C*). Fig. 5*D* demonstrates that unlabeled fibrils become fluorescent, suggesting that amyloid aggregates act as recruitment points for soluble protein, potentially allowing cell-mediated amyloid fibril elongation. Fig. 5*E* describes how this behavior increased over time for each condition examined. No significant differences were observed between the V_L and FL proteins, suggesting that the presence of the C_L domain did not significantly affect amyloid fibril elongation. However, AL-09 FL soluble protein showed a delayed seeding effect (24 h). The three other proteins showed clear seeding after 8 h of co-incubation (Fig. 5*E*). Confocal microscopy experiments using ^{OG}AL-09 V_L co-incubated with Texas Red-labeled fibrils in AC16 cells (not co-transfected with RFP protein) corroborated the co-localization of soluble AL-09 with the fibrils (supplemental Fig. S2).

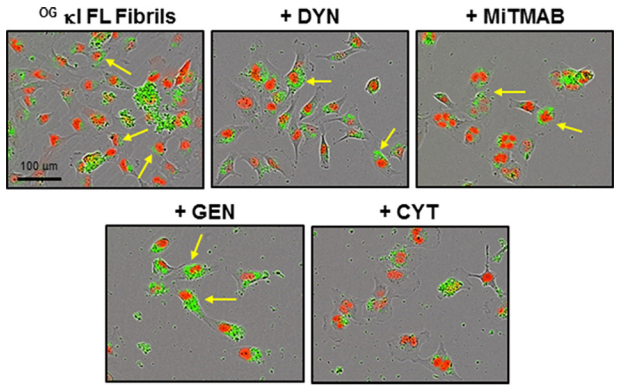

FIGURE 4. **LC fibrils internalize into AC16 through macropinocytosis.** Representative images of AC16 cells after 28 h of co-incubation of 1 μM $^{OG}\kappa$I FL in the presence of 50 μM DYN, 10 μM MiTMAB, 50 μM GEN, or 1 μM CYT. In all cases, external aggregates surround the cardiomyocytes. A fraction of them appear to be internalized (*yellow arrows*) except for those incubated with CYT, where intracellular green fluorescence is practically nonexistent, indicating that fibril macropinocytic internalization is inhibited.

LC Fibrils Are Toxic to AC16 Human Cardiomyocytes—We next tested the toxicity of both soluble proteins and amyloid fibrils in AC16 human cardiomyocytes. For these experiments, we included two more recombinant AL patient-derived proteins: AL-T05 V_L and rVλ6Wil proteins (hereafter called Wil for simplicity), belonging to the Vλ1 1b (IGLV 1–51) and Vλ6 6a (IGLV 6–57) LC family, respectively. AL-T05 V_L has the fastest fibril formation kinetics of all

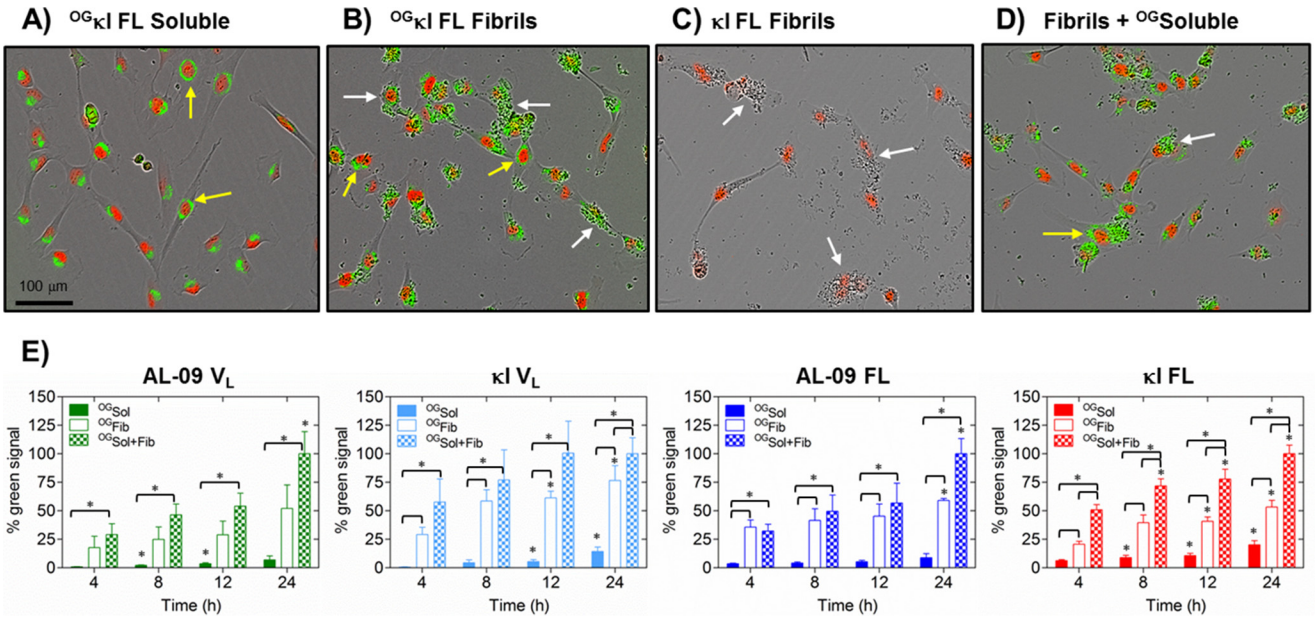

FIGURE 5. **External LC amyloid fibrils act as a seeding point for soluble protein.** *A–C*, representative images comparing AC16 cells after 24 h of incubation with 1 μM ^{OG}κI FL protein (*A*), 1 μM ^{OG}fibrils (*B*), or 1 μM unlabeled fibrils (*C*). *D*, competition experiments with 1 μM unlabeled κI FL fibrils co-incubated with 1 μM ^{OG}soluble LC. Co-localization of ^{OG}soluble LC with unlabeled fibrils causes the latter to become fluorescent, indicating a cell-mediated seeding. *E*, quantification of seeding effect describes how this behavior increases over time for each condition studied. The presence of the CL domain (FL proteins) does not affect the fibril elongation. *Yellow arrows* indicate internalized ^{OG}soluble protein or ^{OG}fibrils, whereas *white arrows* indicate external aggregates attached to cell membrane. Samples were set up in triplicate in three independent assays ($n = 3$) with the average values and *error bars* as means ± S.E. *, two-tailed *t* test; *p* value < 0.05 with respect to the corresponding controls. #, two-tailed *t* test; *p* value < 0.05 between values at same condition.

proteins tested in our laboratory (32); Wil has been extensively studied by Wall *et al.* (33, 34). Wil fibrils have been recently identified to cause metabolic dysfunction in AC10 human cardiomyocytes (24).

Fig. 6 shows the effect of soluble and amyloid fibrils on RFP-AC16 human cardiomyocyte growth rates. At concentrations of 1 and 12 μM, soluble protein had no effect on cell growth rates (Fig. 6, *A* and *B*). Supernatant fractions of fibril formation reactions (which may contain oligomeric species or soluble aggregates) do not have any toxic effect on cells (data not shown). In contrast, fresh κI V_L and Wil 1 μM fibrils (monomer equivalent concentration) prevented cell growth over 80 h of analysis; however, the other variants had no apparent effect on cell growth (Fig. 6*C*).

We next examined the effect of fibril kinetic stability on cell growth of AC16 cardiomyocytes. Incubation of fibrils at 4 °C, followed by a freeze/thawing cycle, showed more inhibition of AC16 cell growth (Fig. 6, *D* and *E*). The FL protein fibrils were generally less inhibitory than their V_L counterparts. The images in the *insets* of Fig. 6 visually demonstrate that RFP-AC16 cell viability decreases with increasing toxicity of AL-09 V_L fibrils, as evidenced by a decrease in cell number (Fig. 6, *C–E*, *insets*). The structure of freshly prepared and incubated fibrils was assessed by transmission electron microscopy (TEM) (Fig. 7). The aggregate morphology is in agreement with what has been published by our laboratory previously, where small clusters of short fibrils aggregate and interact in large conglomerates, the only difference is that we are presenting low resolution images (for representative high resolution images of these aggregates, please review Ref. 65). Distinct morphological and apparent concentration differences are clearly seen between fresh and mature fibrils, which may explain the differences in cell toxicity. Freshly prepared fibrils formed large clusters of aggregates that broke up into smaller clusters over the incubation at 4 °C and the freeze/thaw cycle. We propose that fibril toxicity changes over time and depends on the size and the level of clustering of the aggregates.

Caspase 3/7 activity was measured in the presence of the soluble protein and fibril-treated AC16 cells (Fig. 8) after 80 h of cell treatment (end point of toxicity experiments; Fig. 8, *A–C*). Cells incubated with 1 μM soluble protein did not undergo apoptosis, as compared with the untreated cells (Fig. 8*A*). This result correlates with the cell growth curves. Cell treatment with 12 μM soluble protein did not affect cell growth (Fig. 6*B*); however, both AL-09 V_L and FL soluble proteins showed a significant increase in caspase activity (Fig. 8*B*). The cells incubated with 1 μM fibrils did not increase their caspase activity (Fig. 8*C*). The decreased caspase activity found for κI and AL-09 V_L domains, AL-T05, and Wil fibrils, compared with control, is directly correlated with the reduced number of cells alive after 80 h of treatment (Fig. 6). Thus, the caspase activity for the highly cytotoxic fibrils was extremely low compared with the both non-toxic FL fibrils confirming the high cytostatic effect of LC fibrils. These results suggest that soluble protein can activate apoptotic events in human cardiomyocytes in a concentration-dependent manner, especially those variants that are more amyloidogenic.

ThT Is Not Able to Detect Cytotoxic Fibrillar Species—Fibrillar Wil was the most toxic species in our studies. Therefore, we conducted a titration study to determine the minimum concentration required to observe a toxic effect in AC16 cells. *In vitro* fibril formation reactions were followed by monitoring the fluorescence intensity of thioflavin T (ThT) dye, which is enhanced when ThT binds to amyloid fibrils (35). The ThT

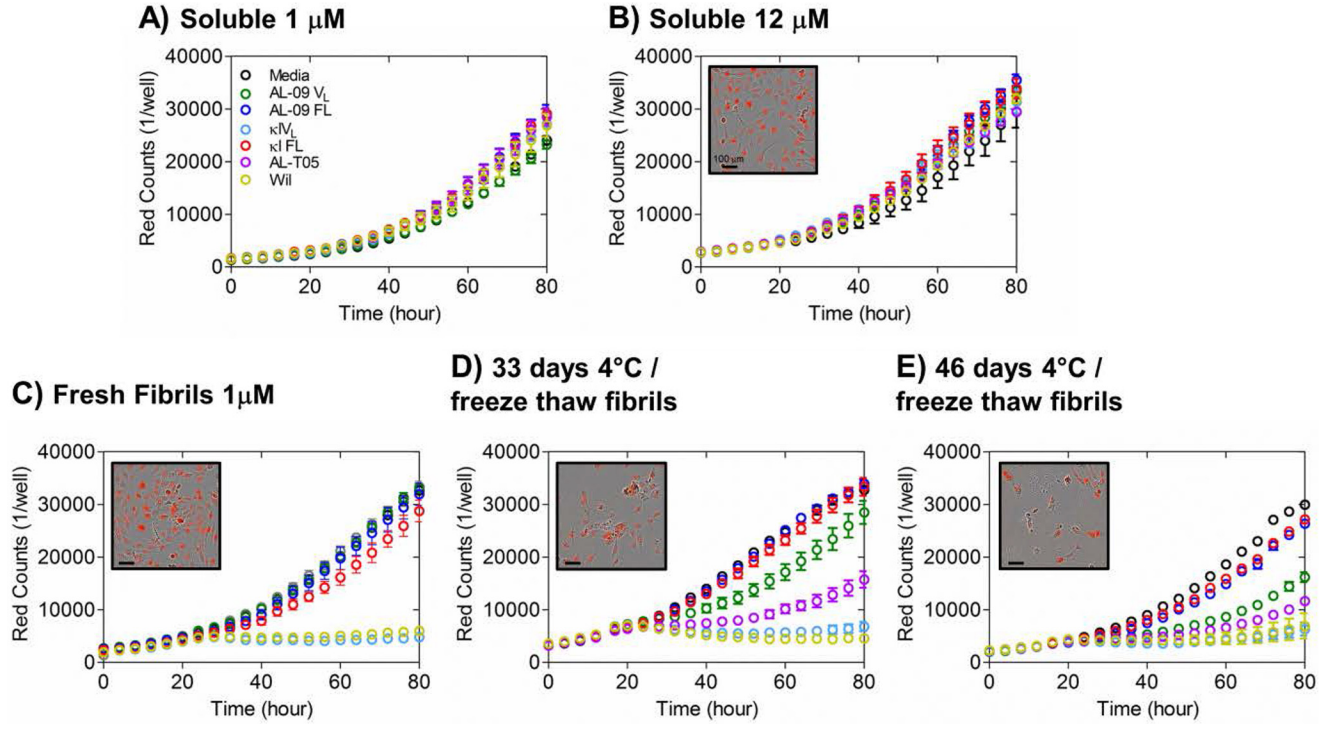

FIGURE 6. **LC fibrils inhibit AC16 cell growth.** *A* and *B*, AC16 cells incubated with soluble proteins at 1 μM (*A*) and 12 μM (*B*) showed no effect on cell growth. *C–E*, AC16 cells incubated with 1 μM amyloid fibrils. Freshly prepared κI V_L and Wil fibrils are highly toxic (*C*). Fibrils composed of AL-09 V_L and AL-T05 increases their effect on cell growth fibrils following incubation at 4 °C (for 33 (*D*) and 46 days (*E*)) followed by a freeze/thaw cycle. FL fibrils slightly increase their cell effect over time. Red fluorescent counts were measured over time and represented the number of adherent RFP-AC16 cell per well. Images in *insets* show representative images of RFP-AC16 cells incubated with AL-09 V_L fibrils (κI FL does not have an effect on cell growth and therefore was not a good representative for these images). Samples were set up in triplicate in four independent assays ($n = 4$) with the average values and *error bars* as means ± S.E.

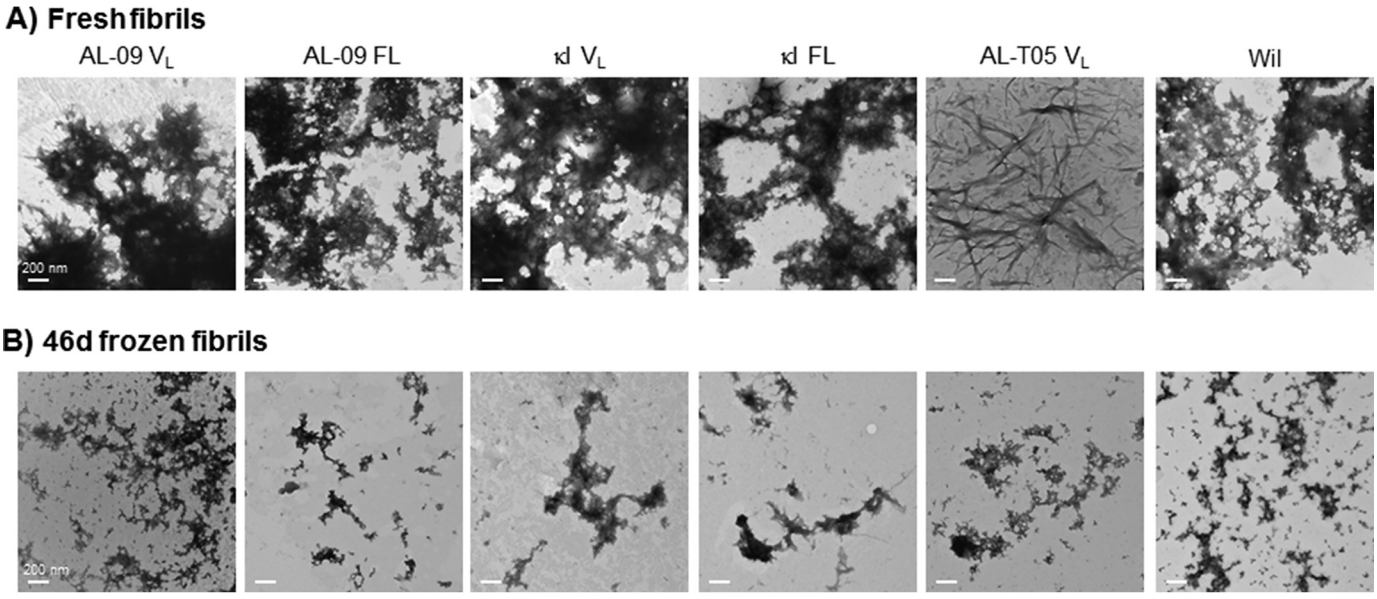

FIGURE 7. **Fresh and incubated LC fibrils show morphological changes.** Transmission electron microscopy images show significant differences between freshly prepared fibrils (*A*) and fibrils incubated at 4 °C for 46 days, after a freeze/thaw cycle (*B*). Fresh fibrils form large complex clusters, whereas mature fibrils appear as smaller aggregates. All fibrils show similar morphological features except for the AL-T05 fresh fibrils, which form an individual fibril mesh instead of the dense matted morphology. All images were taken at 46,000×. The *scale bars* represent 200 nm.

fluorescence emission decreased as a function of fibril concentration (Fig. 9*A*). We grew RFP-AC16 cells in the presence of the dilution series of Wil fibrils (Fig. 9*B*). We observed a decrease in cell growth at the highest concentrations of Wil fibrils. Fig. 9*C* shows that ThT fluorescence signal and percentage of cell growth intersect between 0.2 and 0.4 μM, where the cells grew 50% with respect to the control and the ThT fluorescence is barely above the buffer baseline. A series of cell images incubated with 1 μM of Wil fibrils showed the effect of fibrils on RFP-AC16 cells from time 0 to 64 h (supplemental Fig. S3).

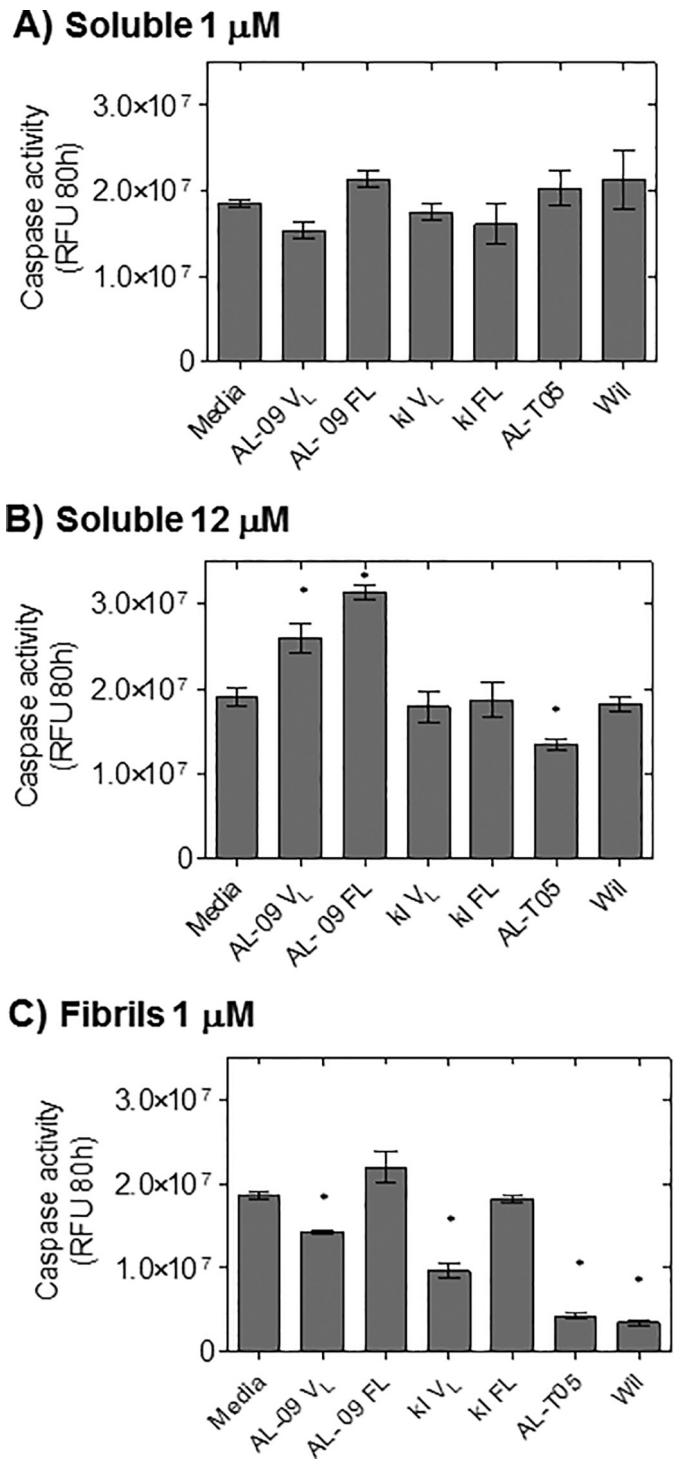

FIGURE 8. **Caspase activity detected in cardiomyocytes cells.** AC16 cells were incubated with 1 μM fibrils (*A*), 12 μM soluble protein (*B*), and 1 μM fibrils (*C*). Apoptosis reagents were added after 80 h of treatment and were incubated for 1 h at 37 °C before reading plate. Caspase activity is indicated as relative fluorescence units (*RFU*). Samples were set up in triplicate in two independent assays ($n = 2$) with the average values and *error bars* as means ± S.E. *, two-tailed *t* test; *p* value < 0.05 with respect to the corresponding media controls.

From these results, we conclude that low ThT signal in fibril formation does not necessarily reflect the absence of toxic fibrillar species and that other fibril detection methods should be employed in addition to ThT fluorescence, particularly at low fibril concentrations.

Discussion

In this study we demonstrate the cellular internalization of LC soluble proteins—AL-09 V_L, FL, κI V_L, and κI FL—and their corresponding amyloid aggregates. Soluble proteins and amyloid fibrils internalize via macropinocytosis. In addition, our results uncover that amyloid fibrils are one of the cytotoxic species responsible for the loss of AC16 cell viability, and the C_L domain modulates AL protein internalization in addition to fibril cytotoxic behavior. We have observed a novel behavior where external aggregates attach to the cells, confine them, and trigger a seeding effect that is significantly accelerated when compared with *in vitro* seeding experiments.

The presence of the C_L domain delays the internalization process, indicating a size-dependent mechanism, as described previously in cardiac fibroblasts (16). The amyloidogenic protein AL-09 internalizes faster than the germline κI, which could be correlated with its lower thermodynamic stability and its higher amyloidogenic propensity (13, 36). Soluble proteins do not accumulate on the plasma membrane. Rather, LC proteins are rapidly internalized into the cardiomyocytes without clear evidence of undergoing a membrane binding step, unlike the findings in human renal mesangial cells (15). Our experiments using endocytic inhibitors exclude any caveolin-mediated pathway for LC internalization. We suggest that the LC proteins tested are taken up into AC16 cardiomyocytes primarily through a macropinocytic pathway. The increased FL protein internalization, found when cells were treated with DYN or GEN, suggested that these inhibitors may favor other internalization pathways. Monis *et al.* (16) also found that CYT inhibits the LC internalization into primary cardiac fibroblasts. Macropinocytosis involves membrane ruffling events that occur in response to actin polymerization near the plasma membrane (37). Macropinosomes fuse with the cellular membrane and are rapidly transported along the endocytic pathway, merging with lysosomal compartments (37, 38), as we reported in mouse HL1 cardiomyocytes (25).

Macropinosomes mediate the cellular internalization of external amyloid aggregates, as has been found in neurodegenerative diseases (39–41). The size of amyloid aggregates would preclude any vesicular endocytosis. The inhibitor effect of MiTMAB suggests a phagocytic mechanism as a secondary pathway for amyloid fibrils internalization (42). Macropinocytosis has also been associated with amyloid transcellular propagation (43). Many studies have reported a cell to cell transfer of misfolded protein and aggregates, triggering the progression of the neurodegenerative disease throughout the brain (39, 40, 44–48). Per Westermark and co-workers (49) have provided evidence that serum amyloid A or secondary amyloidosis (AA) is a transmissible disease. In our study, we described an excretion mechanism by which the internalized protein decreases over time. Protein excretion may depend on low extracellular protein concentration. Gupta and Knowlton (50) first described the release of exosomes by human cardiomyocytes. In the context of amyloid propagation, exosomes are involved in transmission of misfolded and aggregated protein, and further, they are capable of entering cells via macropinocytosis (51, 52).

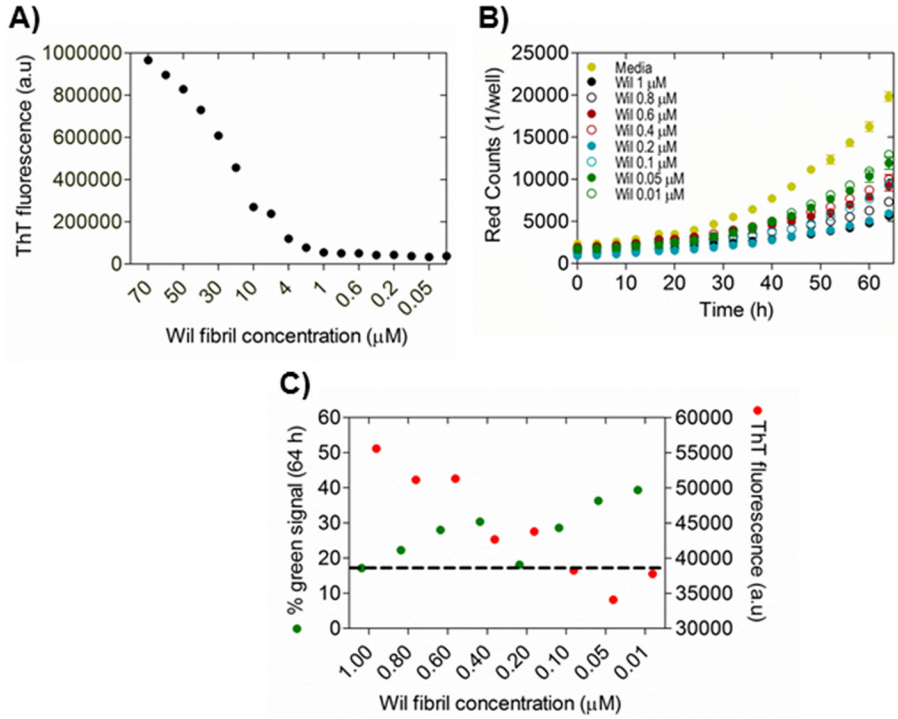

FIGURE 9. **ThT detection of cytotoxic fibrillar species.** *A*, ThT fluorescence decreased as a function of fibril concentration. *B*, cell toxicity experiments with a dilution series of Wil fibrils from 1 to 0.001 μM. Red counts were registered over time as a number of RFP-AC16 cells per well. AC16 growth rate decreases as Wil fibril concentration increases. *C*, plot of cell toxicity *versus* ThT signal. ThT fluorescence is barely above the buffer ThT baseline (*black dashed line*) when cells grow 50% with respect to the control. ThT fluorescence signal and percentage of cell growth intersect between 0.2 and 0.4 μM.

Amyloid fibrils have been considered to play a secondary role in cell toxicity, yielding the toxic role to the soluble species (12, 13, 53). LC fibrillary species were not considered in the toxicity landscape of AL amyloidosis until recently (24). Here we demonstrated the high cytotoxic potential of LC amyloid fibrils when incubated with AC16 cardiomyocytes. Interestingly, we observed a different mechanism of cell toxicity followed by amyloid fibrils and soluble protein. Whereas the LC amyloid fibrils exhibit an efficient inhibition of the cell growth and division, the LC soluble proteins allow cell growth but cause cell dysfunction and apoptosis in AC16 cardiomyocytes. The toxicity potential of both AL-09 VL and FL soluble LC could be correlated with their higher amyloidogenic propensity and faster cell internalization rate compared to the germline κI LC. We confirmed that the concentration of monomeric species within the fibril sample did not increase as the cell viability diminished (using the fibril sedimentation assay reported by Wetzel and co-workers (54)), excluding any reversible fibril process that will shift the equilibrium toward formation of cytotoxic soluble species (data not shown).

The cytotoxic effect of amyloid fibrils increases as they age. TEM images clearly show morphological changes between fresh and aged fibrils, which may explain the differences in cell toxicity. Fragmented amyloid fibrils possess an enhanced cytotoxic potential when compared with longer fibrils (55–57). We propose that fibril toxicity changes over time as fibrils fragment into smaller fibril clusters, which could be related to the ease at which macropinosomes engulf aggregates into cardiomyocytes. This behavior is also in agreement with the possibility that certain amyloid fibril structures may be more pathogenic than others in Alzheimer's disease (58). Fibril size, arrangement, and conformation open the question about whether or not fibril toxicity is dependent on cell internalization and whether CYT would be able to inhibit such cytotoxicity.

LC fibril toxicity could also be correlated with their strong attraction for the plasma membrane, causing a particular cell confinement. Cells surrounded by fibrils are likely to be excluded from cell-cell contact, a vital mechanism for maintaining cell viability. Cell treatment with trypsin (40, 48, 59), chondroitinase ABC, and heparinase II (60, 61) did not detach the external amyloid from the cell membrane (data not shown). We propose that membrane surfaces facilitate fibril attachment and act as an anchor point for cell-mediated seeding mechanism. Extracellular soluble protein would interact with amyloid aggregates on the cellular surroundings.

In vitro seeded acceleration of protein fibrillation has been reported in many proteins (62, 63). We previously demonstrated that the presence of preformed aggregates *in vitro* accelerate the fibril formation reaction (64, 65). In this study we observed soluble protein recruitment to amyloid fibrils in half the time observed *in vitro*, which leads us to propose that seeding is significantly accelerated in a cell culture environment. Because fibrils are highly toxic to cells, the seeding mechanism deserves attention, because it could become an exponential trigger of cell toxicity, propagating fibril elongation throughout the cellular environment.

Future studies including other amyloidogenic LC proteins both in the V_L and FL forms will be necessary to confirm our observations and strengthen the proposed mechanisms of internalization and toxicity observed in this initial study. Our results suggest that AL amyloid internalization, propagation, seeding, and toxicity mechanisms, as well as the role of CL

domains on LC proteins, are correlated, deserving more attention for further studies in AL amyloidosis.

Experimental Procedures

Protein Preparation—The V_L sequences for κI O18/O8 and AL-09 were deposited previously under GenBank™ accession numbers EF640313 and AF490909, respectively (36). There is only one κ C_L sequence (protein accession number P01834). V_L domains and FL proteins were expressed and purified as previously described (25, 36). κI FL sequence was mutated at position C214S (end of C_L domain) to avoid the formation of non-native disulfide bonds. Alternatively, the Cys^{214} position was kept for AL-09 FL because it displayed a better protein expression and higher extraction yield without changing any other biochemical and biophysical properties. Briefly, V_L domains were expressed in *Escherichia coli* BL21 (DE3) Gold competent cells. κI O18/O8 V_L was extracted from the periplasmic space by breaking the cells through one freeze-thaw cycle using PBS buffer, pH 7.4. AL-09 V_L was extracted from solubilized inclusion bodies using 5 M urea and refolded by dialysis against 10 mM Tris-HCl, pH 7.4. FL proteins were expressed in *E. coli* Rosetta Gami competent cells. AL-09 and κI FL were extracted from solubilized inclusion bodies using 5 M urea and refolded by dilution (1:10) in ice-cold refolding buffer (10 mM Tris/HCl, 1 M L-arginine, 7 mM GSH, 0.7 mM GSSG, 2.5 mM EDTA, and 1 mM PMSF protease inhibitor, pH 8.5) for 48 h at 4 °C. All proteins were purified using size exclusion chromatography in 10 mM Tris buffer, pH 7.0, at 4 °C (HiLoad 16/60 Superdex 75 column) on an AKTA FPLC (GE Healthcare). Eluted fractions were checked by SDS-PAGE, and their protein concentration was determined by UV absorption at 280 nm using an extinction coefficient (ϵ) calculated from the amino acid sequence (14,890 and 25,940 $cm^{-1}\ M^{-1}$ for κI VL and FL proteins, respectively; 13,610 and 24,660 $cm^{-1}\ M^{-1}$ for AL-09 VL and FL proteins, respectively). Far UV CD scan and thermal unfolding were obtained as a protein quality control. Proteins were aliquoted at concentration below 100 μM, flash frozen, and stored at −80 °C. Proteins were thawed at 4 °C, filtered, and/or ultracentrifuged before they were used for each study.

Amyloid Fibril Formation—Because the presence of preformed aggregates may accelerate the fibril formation kinetics, protein samples were ultracentrifuged prior to the fibril formation assay following the protocol described by DiCostanzo *et al.* (66). Fibril formation assays were performed in triplicate using black 96-well polystyrene plates and shaken continuously at 300 rpm at 37 °C in a New Brunswick Scientific Innova40 incubator shaker. Each well contained 260 μl of 20 μM protein, 150 mM NaCl, 10 μM thioflavin T (Sigma-Aldrich), 0.02% NaN_3 in 10 mM sodium acetate, boric acid, and sodium citrate (ABC) buffer at pH 2.0 or 3.0 for V_L domains and FL proteins, respectively. These fibril formation solution conditions were chosen because they are the only conditions in which all proteins (V_L and FL) form fibrils with similar morphologies. Making fibrils under physiological solution conditions (pH 7.4) was not a possibility because κI V_L does not form fibrils under those conditions, and κI FL forms a mixture of amorphous aggregates with amyloid fibrils at that pH. ThT fluorescence was used to follow the fibril formation kinetics (67, 68) and was monitored daily on a plate reader (Analyst AD; Molecular Devices, Sunnyvale, CA) with an excitation wavelength of 440 nm and an emission wavelength of 480 nm, until the reaction reached the plateau (~600–800 h). A fibril formation reaction was considered completed when ThT fluorescence enhancement reached a plateau and was considered positive when ThT fluorescence readings reached at least four times the lowest ThT reading of that particular reaction (usually 200,000 counts/s). Fibrils were washed in PBS, pH 7.4, and stored at 4 °C until they were used in cell culture.

Oregon Green Soluble Protein Conjugation—Oregon Green 488 (Invitrogen) conjugation reactions were conducted as reported by Levinson *et al.* (25). Protein samples were thawed at 4 °C. Tris buffer was exchanged to PBS using a 10,000 molecular weight cutoff centrifugal filter units (Millipore, Billerica, MA). 200–500 μl of protein solution was used in each labeling reaction, at a concentration of <2 mg/ml. 100 mM $NaHCO_3$, pH 8.5, was added to each protein sample to raise the pH of the reaction mixture. 1 mg of OG was solubilized in 100 μl of DMSO (10 mg/ml). The volume of OG dye stock solution to be added was calculated as follows.

$$\text{OG stock solution } (\mu l) = [(\text{mg/ml protein} \times \text{ml protein})/\text{Mr protein}] \times \text{Mr OG} \times \text{CF} \times \text{MR} \quad \text{(Eq. 1)}$$

The molecular weight (M_r) of the proteins used was as follows: 11,930 and 23,504 g/mol for both VL domain and both FL proteins, respectively. The M_r of OG is 509 g/mol, the conversion factor (CF) is 100, and the molar ratio (MR) of dye to protein in the reaction mixture is 20.

Soluble proteins were labeled overnight at 4 °C, protected from light. Free OG was removed from the soluble labeled protein by consecutive rounds of protein concentration and dilution with PBS, pH 7.4, through a 10,000 molecular weight cutoff centrifugal filter. Samples were then filtered using a 0.45 μm filter and the protein concentration and degree of labeling were calculated by the following formula,

$$\text{Protein concentration (mol/l)} = [Abs_{280} - (Abs_{496} \times 0.12) \times DF]/\epsilon\text{-protein} \quad \text{(Eq. 2)}$$

where *DF* is the dilution factor (when applied), 0.12 is a correction factor to account for absorption of the dye at 280 nm. ϵ-Protein is the molar extinction coefficient of each protein (14,890 and 25,940 $M^{-1}\ cm^{-1}$ for κI O18/O8 VL and FL proteins, respectively; 13,610 and 24,660 $M^{-1}\ cm^{-1}$ for AL-09 VL and FL proteins, respectively); ϵ-OG is the molar extinction coefficient of OG (70,000 $M^{-1}\ cm^{-1}$).

Oregon Green Amyloid Conjugation—At the end of fibril formation reaction, fibrils were collected, pelleted, and washed three times with PBS buffer by centrifugation at 14,000 rpm, 5 min at room temperature. 200–500 μl of PBS resuspended fibrils were used in each labeling reaction, at a concentration range of 0.5–1 mg/ml. Fibrils were incubated with OG for 2 h at room temperature, protected from light. Free OG was removed from labeled fibrils by centrifugation. Supernatant

was removed and quantified to determine the concentration of soluble protein left after fibril formation. Final fibril concentration was adjusted to that number. The degree of labeling was determined for each conjugation as described for the soluble proteins and used to normalize the fluorescence intensities of cellular experiments.

Cell Culture—AC16 human primary ventricular cardiomyocytes were purchased from Dr. Mercy Davidson at Columbia University. This cell line has been immortalized by fusion with SV40 transformed fibroblast cell line devoid of mitochondrial DNA (69). The cells were maintained with DMEM/F12 medium (Life Technologies Inc.) supplemented with 12.5% FBS (Mediatech, Manassas, VA) and 1% penicillin/streptomycin (Invitrogen). AC16 cells co-transfected with plasmid expressing RFP in the nucleus were also used (RFP-AC16 cells). For the nuclear cell labeling, the IncuCyte^{TM} NucLight^{TM} lentivirus reagent has been used (Essen Bioscience). NucLight Lentiviruses drive the expression of nuclear localization signal-tagged fluorescent proteins with an EF-1α promoter. The NucLight red version expresses mKate2 in the nucleus of the cells. Cell culture experiments were carried out under sterile conditions. AC16 cells are not listed in the database of commonly misidentified cell lines maintained by ICLAC. As a control of viability and differentiation, cell morphology was always checked before each experiment, and the number of cell passages after thawing was limited to 20.

Cell Internalization Experiments—Internalization experiments were carried out using the IncuCyte ZOOM (Essen Bioscience, Ann Arbor, MI) incubator. The microscope incorporated into the incubator supports two different fluorescence channels. We took advantage of the two color setup and used RFP-AC16 cells incubated with soluble proteins or fibrillar aggregates conjugated with OG dye (^{OG}AL-09 V_L, FL, and $^{OG}\kappa$I V_L, FL).

AC16 cardiomyocytes were plated at a concentration of 2,000 cells/well (10,000 cells/ml) in a 96-well Corning polystyrene plate and allowed to grow overnight (<20 h) into the IncuCyte ZOOM incubator (5% CO_2 at 37 °C) for cell attachment. 200 μl of cell culture medium was replaced with 100 μl of fresh medium. 100 μl of ^{OG}soluble LC or ^{OG}fibrils were added to the cells at a final concentration of 1 μM. To assess the effect of amyloid fibrils on the protein internalization process, the cells were co-incubated with ^{OG}soluble LC mixed with non-labeled fibrils, at a ratio of 1:1. Plates were scanned every 4 h. Internalization data were collected 4, 8, 12, and 24 h after addition of the protein. For this, 10 min before the desired time point, cell medium-containing ^{OG}soluble LC/fibrils were replaced with free fresh medium to remove the fraction not internalized. Red (RPF-AC16) and green (^{OG}soluble LC/fibrils) fluorescence channels were selected, and 5% of the red signal was removed from the green signal to avoid spectral mixing. A four-field scan pattern was used for each well, and the average data were collected as a green counts or red counts per well. Each condition was set up in triplicate. For a correct comparison between different AL proteins, green fluorescence intensities were normalized for each protein as a function of their degree of labeling determined after each conjugation as described above.

After 24 h, the cell medium-containing ^{OG}soluble LC/fibrils of three 200-μl wells was replaced with free fresh medium. The cells were scanned every 4 h for a longer period of time, which allowed us to follow the decrease of intracellular soluble protein. After 48 h, the media of three different 200-μl wells were replaced and also scanned every 4 h. The fluorescence intensity of the two different time sets helped us to discern between a quenching effect and secretion mechanism.

To remove the extracellular aggregates, cells were incubated with 0.01% or 0.5% trypsin-EDTA (Life Technologies Inc.) in DMEM/F12 medium for 2 min and washed with DMEM/F12 medium for deactivation of the trypsin. The cells were also incubated with chondroitinase ABC and heparinase II (Sigma-Aldrich) at 12.5, 6.25, and 3.12 milliunits/ml in DMEM/F12 medium for 1 h at 37 °C. Because of our inability to detach the fibrils from the cell membrane, we were unable to quantify the amount of fibrils internalized into AC16 cells.

Protein Internalization Inhibition Assays—Prior to soluble protein internalization assay, RFP-AC16 cells were incubated for 30 min at 37 °C with 50 μM DYN, 10 μM MiTMAB, 50 μM GEN, or 1 μM CYT. Thereafter, ^{OG}soluble LC/fibrils were added to the cells and followed throughout time in presence of inhibitor. The data were collected as described above. Green counts and red counts per well in the presence of inhibitor were compared with the data in the absence of inhibitors.

Cell Viability Assays—Experimental setup was followed as described for the internalization experiments, except that both proteins and fibrils were unconjugated. RFP-AC16 cells were incubated with 1 or 12 μM of soluble protein, or with 1 μM of amyloid fibrils. Fibrils are stored at 4 °C after the fibril formation reaction is completed. Freeze/thawing cycles has been done before each experiment in all cases except the experiments using fresh fibrils. The changes in cell growth were followed by red counts per well (or percentages of red cells per well) every 4 h until cells become over confluent (>80 h).

The apoptotic index has been assessed by using the homogeneous caspase assay fluorimetric kit (Roche). We first used the apoptotic reagent CellPlayer^{TM} kinetic caspase-3/7 (Essen Bioscience) for use on the IncuCyte ZOOM^{TM} imaging systems, which kinetically quantify cell proliferation over time in a non-perturbing way. Unexpectedly, the apoptotic reagent binds to the external amyloid aggregates, releasing green fluorescent signal. To avoid false positives, we used the caspase assay kit. In brief, at the end of the cell viability assays (80 h), 100 μl of substrate working solution was added to each well and incubated for 1 h at 37 °C, 5% CO_2. The plate was read on the Analyst AD plate reader (Molecular Devices) at an excitation wavelength of 480 nm and an emission wavelength of 520 nm, medium attenuator mode, and continuous lamp. The average data were collected as relative fluorescence units/well. Each condition was set up in triplicate, and each well was read three times.

Transmission Electron Microscopy—Amyloid fibril morphologies were confirmed by transmission electron microscopy. A 5-μl fibril sample was placed on a 300-mesh copper Formvar/carbon grid (Electron Microscopy Science, Hatfield, PA), and excess liquid was removed. The samples were negatively stained with 4% uranyl acetate, washed once with sterile H_2O,

and air-dried. Grids were analyzed on a Philips Tecnai T12 transmission electron microscope at 80 kV (FEI, Hillsboro, OR).

Confocal Microscopy—For co-localization experiments with ^{OG}soluble LC and Texas Red-labeled fibrils, the AC16 cardiomyocytes used were not co-transfected with RFP protein (no red nucleus). the Cells were previously fixed with 4% paraformaldehyde-PBS solution for 30 min at room temperature. An LSM 780 confocal microscope (Carl Zeiss Microscopy) was used to image the cells with a 40× differential interference contrast lens using a water immersion objective (Zen software). Laser wavelengths of 488 and 561 nm were used. For *Z* stacks series, 15 slices that were 0.5 mm thick were taken. The images were captured using Zeiss LSM Image version 3.2SP2. Images were collected with ×4 averaging. Detector gain and amplitude offset were determined for each experiment to maximize the linear range without saturation and were kept consistent for comparable experiments. The images were prepared using ImageJ.

Determination of Monomer Concentration by Reverse Phase HPLC Assay—Quantification of monomer concentration on fibril supernatant samples was performed using a HPLC sedimentation assay as previously described (54). Briefly, a 100-μl fibril sample in 10 mM ABC buffer, pH 2.0 or 3.0 (see "Amyloid Fibril Formation") was taken before each fibril toxicity experiments. Before injection into the analytical reverse phase HPLC chromatography (BioLogic DuoFlow Pathfinder 20 system), samples were ultracentrifuged at 90,000 rpm for 45 min at room temperature to remove aggregates. 70-μl supernatant fractions were injected into a C8 column to determine the concentration of monomers and eluted by a linear gradient of acetonitrile in aqueous 0.05 TFA. The area under the curve of the chromatography peak at specific retention time was integrated, and the concentration was determined from a standard curve done for each AL protein.

Author Contributions—M. M.-A. designed the experiments, performed the experiments, analyzed the data, and wrote the paper. Y. L. designed the experiments and revised the manuscript. P. M. performed the HPLC experiments. A. W., L. R. E., and M. M. performed the experiments. J. S. W. revised the manuscript. K. G. H. assisted with experiments and processed data. M. R.-A. designed the experiments, analyzed the data, wrote the paper, revised the manuscript, and gave final approval.

Acknowledgments—We thank Shaun G. Weller, Eugene W. Krueger, and Ramirez-Alvarado team members for helpful discussion and critical reading of this manuscript. We especially thank Dr. Allan B. Dietz for letting us the access to the IncuCyteZOOM™ imaging system. We are also thankful for the generosity of amyloidosis patients and their families.

References

1. Baden, E. M., Sikkink, L. A., and Ramirez-Alvarado, M. (2009) Light chain amyloidosis: current findings and future prospects. *Curr. Protein Pept. Sci.* **10,** 500–508
2. Falk, R. H. (2005) Diagnosis and management of the cardiac amyloidoses. *Circulation* **112,** 2047–2060
3. Kumar, S. K., Gertz, M. A., Lacy, M. Q., Dingli, D., Hayman, S. R., Buadi, F. K., Short-Detweiler, K., Zeldenrust, S. R., Leung, N., Greipp, P. R., Lust, J. A., Russell, S. J., Kyle, R. A., Rajkumar, S. V., and Dispenzieri, A. (2011) Recent improvements in survival in primary systemic amyloidosis and the importance of an early mortality risk score. *Mayo Clin. Proc.* **86,** 12–18
4. Glenner, G. G., Cuatrecasas, P., Isersky, C., Bladen, H. A., and Eanes, E. D. (1969) Physical and chemical properties of amyloid fibers: II. Isolation of a unique protein constituting the major component from human splenic amyloid fibril concentrates. *J. Histochem. Cytochem.* **17,** 769–780
5. Olsen, K. E., Sletten, K., and Westermark, P. (1998) Fragments of the constant region of immunoglobulin light chains are constituents of AL-amyloid proteins. *Biochem. Biophys. Res. Commun.* **251,** 642–647
6. Vrana, J. A., Gamez, J. D., Madden, B. J., Theis, J. D., Bergen, H. R., 3rd, and Dogan, A. (2009) Classification of amyloidosis by laser microdissection and mass spectrometry-based proteomic analysis in clinical biopsy specimens. *Blood* **114,** 4957–4959
7. Lavatelli, F., Perlman, D. H., Spencer, B., Prokaeva, T., McComb, M. E., Théberge, R., Connors, L. H., Bellotti, V., Seldin, D. C., Merlini, G., Skinner, M., and Costello, C. E. (2008) Amyloidogenic and associated proteins in systemic amyloidosis proteome of adipose tissue. *Mol. Cell. Proteomics* **7,** 1570–1583
8. Sethi, S., Vrana, J. A., Theis, J. D., Leung, N., Sethi, A., Nasr, S. H., Fervenza, F. C., Cornell, L. D., Fidler, M. E., and Dogan, A. (2012) Laser microdissection and mass spectrometry-based proteomics aids the diagnosis and typing of renal amyloidosis. *Kidney Int.* **82,** 226–234
9. Klimtchuk, E. S., Gursky, O., Patel, R. S., Laporte, K. L., Connors, L. H., Skinner, M., and Seldin, D. C. (2010) The critical role of the constant region in thermal stability and aggregation of amyloidogenic immunoglobulin light chain. *Biochemistry* **49,** 9848–9857
10. Blancas-Mejía, L. M., Horn, T. J., Marin-Argany, M., Auton, M., Tischer, A., and Ramirez-Alvarado, M. (2015) Thermodynamic and fibril formation studies of full length immunoglobulin light chain AL-09 and its germline protein using scan rate dependent thermal unfolding. *Biophys. Chem.* **207,** 13–20
11. Brenner, D. A., Jain, M., Pimentel, D. R., Wang, B., Connors, L. H., Skinner, M., Apstein, C. S., and Liao, R. (2004) Human amyloidogenic light chains directly impair cardiomyocyte function through an increase in cellular oxidant stress. *Circ. Res.* **94,** 1008–1010
12. Shi, J., Guan, J., Jiang, B., Brenner, D. A., Del Monte, F., Ward, J. E., Connors, L. H., Sawyer, D. B., Semigran, M. J., Macgillivray, T. E., Seldin, D. C., Falk, R., and Liao, R. (2010) Amyloidogenic light chains induce cardiomyocyte contractile dysfunction and apoptosis via a non-canonical p38α MAPK pathway. *Proc. Natl. Acad. Sci. U.S.A.* **107,** 4188–4193
13. Sikkink, L. A., and Ramirez-Alvarado, M. (2010) Cytotoxicity of amyloidogenic immunoglobulin light chains in cell culture. *Cell Death Dis.* **1,** e98
14. Trinkaus-Randall, V., Walsh, M. T., Steeves, S., Monis, G., Connors, L. H., and Skinner, M. (2005) Cellular response of cardiac fibroblasts to amyloidogenic light chains. *Am. J. Pathol.* **166,** 197–208
15. Teng, J., Russell, W. J., Gu, X., Cardelli, J., Jones, M. L., and Herrera, G. A. (2004) Different types of glomerulopathic light chains interact with mesangial cells using a common receptor but exhibit different intracellular trafficking patterns. *Lab. Invest.* **84,** 440–451
16. Monis, G. F., Schultz, C., Ren, R., Eberhard, J., Costello, C., Connors, L., Skinner, M., and Trinkaus-Randall, V. (2006) Role of endocytic inhibitory drugs on internalization of amyloidogenic light chains by cardiac fibroblasts. *Am. J. Pathol.* **169,** 1939–1952
17. Fändrich, M. (2012) Oligomeric intermediates in amyloid formation: structure determination and mechanisms of toxicity. *J. Mol. Biol.* **421,** 427–440
18. Haass, C., and Selkoe, D. J. (2007) Soluble protein oligomers in neurodegeneration: lessons from the Alzheimer's amyloid β-peptide. *Nat. Rev. Mol. Cell Biol.* **8,** 101–112
19. Kayed, R., Head, E., Thompson, J. L., McIntire, T. M., Milton, S. C., Cotman, C. W., and Glabe, C. G. (2003) Common structure of soluble amyloid oligomers implies common mechanism of pathogenesis. *Science* **300,** 486–489
20. Glabe, C. G. (2008) Structural classification of toxic amyloid oligomers. *J. Biol. Chem.* **283,** 29639–29643

21. Engel, M. F., Khemtémourian, L., Kleijer, C. C., Meeldijk, H. J., Jacobs, J., Verkleij, A. J., de Kruijff, B., Killian, J. A., and Höppener, J. W. (2008) Membrane damage by human islet amyloid polypeptide through fibril growth at the membrane. *Proc. Natl. Acad. Sci. U.S.A.* **105,** 6033–6038
22. Gharibyan, A. L., Zamotin, V., Yanamandra, K., Moskaleva, O. S., Margulis, B. A., Kostanyan, I. A., and Morozova-Roche, L. A. (2007) Lysozyme amyloid oligomers and fibrils induce cellular death via different apoptotic/necrotic pathways. *J. Mol. Biol.* **365,** 1337–1349
23. Kieninger, B., Eriksson, M., Kandolf, R., Schnabel, P. A., Schönland, S., Kristen, A. V., Hegenbart, U., Lohse, P., and Röcken, C. (2010) Amyloid in endomyocardial biopsies. *Virchows Arch.* **456,** 523–532
24. McWilliams-Koeppen, H. P., Foster, J. S., Hackenbrack, N., Ramirez-Alvarado, M., Donohoe, D., Williams, A., Macy, S., Wooliver, C., Wortham, D., Morrell-Falvey, J., Foster, C. M., Kennel, S. J., and Wall, J. S. (2015) Light chain amyloid fibrils cause metabolic dysfunction in human cardiomyocytes. *PLoS One* **10,** e0137716
25. Levinson, R. T., Olatoye, O. O., Randles, E. G., Howell, K. G., DiCostanzo, A. C., and Ramirez-Alvarado, M. (2013) Role of mutations in the cellular internalization of amyloidogenic light chains into cardiomyocytes. *Sci. Rep.* **3,** 1278
26. Newton, A. J., Kirchhausen, T., and Murthy, V. N. (2006) Inhibition of dynamin completely blocks compensatory synaptic vesicle endocytosis. *Proc. Natl. Acad. Sci. U.S.A.* **103,** 17955–17960
27. Macia, E., Ehrlich, M., Massol, R., Boucrot, E., Brunner, C., and Kirchhausen, T. (2006) Dynasore, a cell-permeable inhibitor of dynamin. *Dev. Cell* **10,** 839–850
28. Kirchhausen, T., Macia, E., and Pelish, H. E. (2008) Use of dynasore, the small molecule inhibitor of dynamin, in the regulation of endocytosis. *Methods Enzymol.* **438,** 77–93
29. Quan, A., McGeachie, A. B., Keating, D. J., van Dam, E. M., Rusak, J., Chau, N., Malladi, C. S., Chen, C., McCluskey, A., Cousin, M. A., and Robinson, P. J. (2007) Myristyl trimethyl ammonium bromide and octadecyl trimethyl ammonium bromide are surface-active small molecule dynamin inhibitors that block endocytosis mediated by dynamin I or dynamin II. *Mol. Pharmacol.* **72,** 1425–1439
30. Joshi, S., Perera, S., Gilbert, J., Smith, C. M., Mariana, A., Gordon, C. P., Sakoff, J. A., McCluskey, A., Robinson, P. J., Braithwaite, A. W., and Chircop, M. (2010) The dynamin inhibitors MiTMAB and OcTMAB induce cytokinesis failure and inhibit cell proliferation in human cancer cells. *Mol. Cancer Ther.* **9,** 1995–2006
31. Mooren, O. L., Galletta, B. J., and Cooper, J. A. (2012) Roles for actin assembly in endocytosis. *Annu. Rev. Biochem.* **81,** 661–686
32. Poshusta, T. L., Katoh, N., Gertz, M. A., Dispenzieri, A., and Ramirez-Alvarado, M. (2013) Thermal stability threshold for amyloid formation in light chain amyloidosis. *Int. J. Mol. Sci.* **14,** 22604–22617
33. Wall, J., Schell, M., Murphy, C., Hrncic, R., Stevens, F. J., and Solomon, A. (1999) Thermodynamic instability of human λ6 light chains: correlation with fibrillogenicity. *Biochemistry* **38,** 14101–14108
34. Wall, J. S., Gupta, V., Wilkerson, M., Schell, M., Loris, R., Adams, P., Solomon, A., Stevens, F., and Dealwis, C. (2004) Structural basis of light chain amyloidogenicity: comparison of the thermodynamic properties, fibrillogenic potential and tertiary structural features of four Vλ6 proteins. *J. Mol. Recognit.* **17,** 323–331
35. Biancalana, M., and Koide, S. (2010) Molecular mechanism of thioflavin-T binding to amyloid fibrils. *Biochim. Biophys. Acta.* **1804,** 1405–1412
36. Baden, E. M., Owen, B. A., Peterson, F. C., Volkman, B. F., Ramirez-Alvarado, M., and Thompson, J. R. (2008) Altered dimer interface decreases stability in an amyloidogenic protein. *J. Biol. Chem.* **283,** 15853–15860
37. Kerr, M. C., and Teasdale, R. D. (2009) Defining macropinocytosis. *Traffic* **10,** 364–371
38. Racoosin, E. L., and Swanson, J. A. (1993) Macropinosome maturation and fusion with tubular lysosomes in macrophages. *J. Cell Biol.* **121,** 1011–1020
39. Münch, C., O'Brien, J., and Bertolotti, A. (2011) Prion-like propagation of mutant superoxide dismutase-1 misfolding in neuronal cells. *Proc. Natl. Acad. Sci. U.S.A.* **108,** 3548–3553
40. Holmes, B. B., DeVos, S. L., Kfoury, N., Li, M., Jacks, R., Yanamandra, K., Ouidja, M. O., Brodsky, F. M., Marasa, J., Bagchi, D. P., Kotzbauer, P. T., Miller, T. M., Papy-Garcia, D., and Diamond, M. I. (2013) Heparan sulfate proteoglycans mediate internalization and propagation of specific proteopathic seeds. *Proc. Natl. Acad. Sci. U.S.A.* **110,** E3138–E3147
41. Tang, W., Tam, J. H., Seah, C., Chiu, J., Tyrer, A., Cregan, S. P., Meakin, S. O., and Pasternak, S. H. (2015) Arf6 controls β-amyloid production by regulating macropinocytosis of the amyloid precursor protein to lysosomes. *Mol. Brain* **8,** 41
42. Gold, E. S., Underhill, D. M., Morrissette, N. S., Guo, J., McNiven, M. A., and Aderem, A. (1999) Dynamin 2 is required for phagocytosis in macrophages. *J. Exp. Med.* **190,** 1849–1856
43. Zeineddine, R., and Yerbury, J. J. (2015) The role of macropinocytosis in the propagation of protein aggregation associated with neurodegenerative diseases. *Front. Physiol.* **6,** 277
44. Frost, B., and Diamond, M. I. (2010) Prion-like mechanisms in neurodegenerative diseases. *Nat. Rev. Neurosci.* **11,** 155–159
45. Kaminski Schierle, G. S., van de Linde, S., Erdelyi, M., Esbjörner, E. K., Klein, T., Rees, E., Bertoncini, C. W., Dobson, C. M., Sauer, M., and Kaminski, C. F. (2011) *In situ* measurements of the formation and morphology of intracellular β-amyloid fibrils by super-resolution fluorescence imaging. *J. Am. Chem. Soc.* **133,** 12902–12905
46. Furukawa, Y., Kaneko, K., Watanabe, S., Yamanaka, K., and Nukina, N. (2013) Intracellular seeded aggregation of mutant Cu,Zn-superoxide dismutase associated with amyotrophic lateral sclerosis. *FEBS Lett.* **587,** 2500–2505
47. Sundaramoorthy, V., Walker, A. K., Yerbury, J., Soo, K. Y., Farg, M. A., Hoang, V., Zeineddine, R., Spencer, D., and Atkin, J. D. (2013) Extracellular wildtype and mutant SOD1 induces ER-Golgi pathology characteristic of amyotrophic lateral sclerosis in neuronal cells. *Cell Mol. Life Sci.* **70,** 4181–4195
48. Michel, C. H., Kumar, S., Pinotsi, D., Tunnacliffe, A., St George-Hyslop, P., Mandelkow, E., Mandelkow, E. M., Kaminski, C. F., and Kaminski Schierle, G. S. (2014) Extracellular monomeric tau protein is sufficient to initiate the spread of tau protein pathology. *J. Biol. Chem.* **289,** 956–967
49. Lundmark, K., Westermark, G. T., Nyström, S., Murphy, C. L., Solomon, A., and Westermark, P. (2002) Transmissibility of systemic amyloidosis by a prion-like mechanism. *Proc. Natl. Acad. Sci. U.S.A.* **99,** 6979–6984
50. Gupta, S., and Knowlton, A. A. (2007) HSP60 trafficking in adult cardiac myocytes: role of the exosomal pathway. *Am. J. Physiol. Heart Circ. Physiol.* **292,** H3052–H3056
51. Grad, L. I., Yerbury, J. J., Turner, B. J., Guest, W. C., Pokrishevsky, E., O'Neill, M. A., Yanai, A., Silverman, J. M., Zeineddine, R., Corcoran, L., Kumita, J. R., Luheshi, L. M., Yousefi, M., Coleman, B. M., Hill, A. F., *et al.* (2014) Intercellular propagated misfolding of wild-type Cu/Zn superoxide dismutase occurs via exosome-dependent and -independent mechanisms. *Proc. Natl. Acad. Sci. U.S.A.* **111,** 3620–3625
52. Fitzner, D., Schnaars, M., van Rossum, D., Krishnamoorthy, G., Dibaj, P., Bakhti, M., Regen, T., Hanisch, U. K., and Simons, M. (2011) Selective transfer of exosomes from oligodendrocytes to microglia by macropinocytosis. *J. Cell Sci.* **124,** 447–458
53. Guan, J., Mishra, S., Qiu, Y., Shi, J., Trudeau, K., Las, G., Liesa, M., Shirihai, O. S., Connors, L. H., Seldin, D. C., Falk, R. H., MacRae, C. A., and Liao, R. (2014) Lysosomal dysfunction and impaired autophagy underlie the pathogenesis of amyloidogenic light chain-mediated cardiotoxicity. *EMBO Mol. Med.* **6,** 1493–1507
54. O'Nuallain, B., Thakur, A. K., Williams, A. D., Bhattacharyya, A. M., Chen, S., Thiagarajan, G., and Wetzel, R. (2006) Kinetics and thermodynamics of amyloid assembly using a high-performance liquid chromatography-based sedimentation assay. *Methods Enzymol.* **413,** 34–74
55. Xue, W. F., Hellewell, A. L., Gosal, W. S., Homans, S. W., Hewitt, E. W., and Radford, S. E. (2009) Fibril fragmentation enhances amyloid cytotoxicity. *J. Biol. Chem.* **284,** 34272–34282
56. Xue, W. F., Hellewell, A. L., Hewitt, E. W., and Radford, S. E. (2010) Fibril fragmentation in amyloid assembly and cytotoxicity: when size matters. *Prion.* **4,** 20–25
57. Lee, Y. J., Savtchenko, R., Ostapchenko, V. G., Makarava, N., and Baskakov, I. V. (2011) Molecular structure of amyloid fibrils controls the relationship between fibrillar size and toxicity. *PLoS One* **6,** e20244

58. Lu, J. X., Qiang, W., Yau, W. M., Schwieters, C. D., Meredith, S. C., and Tycko, R. (2013) Molecular structure of β-amyloid fibrils in Alzheimer's disease brain tissue. *Cell* **154,** 1257–1268
59. Kameyama, S., Horie, M., Kikuchi, T., Omura, T., Tadokoro, A., Takeuchi, T., Nakase, I., Sugiura, Y., and Futaki, S. (2007) Acid wash in determining cellular uptake of Fab/cell-permeating peptide conjugates. *Biopolymers* **88,** 98–107
60. Calvet, C. M., Toma, L., De Souza, F. R., Meirelles Mde, N., and Pereira, M. C. (2003) Heparan sulfate proteoglycans mediate the invasion of cardiomyocytes by *Trypanosoma cruzi*. *J. Eukaryot. Microbiol.* **50,** 97–103
61. Potter, K. J., Werner, I., Denroche, H. C., Montane, J., Plesner, A., Chen, Y., Lei, D., Soukhatcheva, G., Warnock, G. L., Oberholzer, J., Fraser, P. E., and Verchere, C. B. (2015) Amyloid formation in human islets is enhanced by heparin and inhibited by heparinase. *Am. J. Transplant* **15,** 1519–1530
62. Andersen, C. B., Yagi, H., Manno, M., Martorana, V., Ban, T., Christiansen, G., Otzen, D. E., Goto, Y., and Rischel, C. (2009) Branching in amyloid fibril growth. *Biophys. J.* **96,** 1529–1536
63. Morales, R., Moreno-Gonzalez, I., and Soto, C. (2013) Cross-seeding of misfolded proteins: implications for etiology and pathogenesis of protein misfolding diseases. *PLoS Pathog.* **9,** e1003537
64. Martin, D. J., and Ramirez-Alvarado, M. (2010) Comparison of amyloid fibril formation by two closely related immunoglobulin light chain variable domains. *Amyloid* **17,** 129–136
65. Blancas-Mejía, L. M., and Ramirez-Alvarado, M. (2016) Recruitment of light chains by homologous and heterologous fibrils shows distinctive kinetic and conformational specificity. *Biochemistry* **55,** 2967–2978
66. DiCostanzo, A. C., Thompson, J. R., Peterson, F. C., Volkman, B. F., and Ramirez-Alvarado, M. (2012) Tyrosine residues mediate fibril formation in a dynamic light chain dimer interface. *J. Biol. Chem.* **287,** 27997–28006
67. Khurana, R., Coleman, C., Ionescu-Zanetti, C., Carter, S. A., Krishna, V., Grover, R. K., Roy, R., and Singh, S. (2005) Mechanism of thioflavin T binding to amyloid fibrils. *J. Struct. Biol.* **151,** 229–238
68. Naiki, H., Higuchi, K., Hosokawa, M., and Takeda, T. (1989) Fluorometric determination of amyloid fibrils in vitro using the fluorescent dye, thioflavin T1. *Anal. Biochem.* **177,** 244–249
69. Davidson, M. M., Nesti, C., Palenzuela, L., Walker, W. F., Hernandez, E., Protas, L., Hirano, M., and Isaac, N. D. (2005) Novel cell lines derived from adult human ventricular cardiomyocytes. *J. Mol. Cell. Cardiol.* **39,** 133–147